International Journal of Industrial Electronics, Control and Optimization IECO
Vol. 4, No. 4, pp. 445-451, Sep (2021)

Determining Optimal Value of Pole Arc to Pole Pitch Ratio to Increase Average Torque and Decrease Unbalance Magnetic Force in Hybrid Electrical Vehicle

Alireza Hoseinpour [1,†] and Ahmad Khajeh[2]

[1]Faculty of Electrical Engineering, University of Zabol, Zabol, Iran
[2] Faculty of Electrical and Computer Engineering, University of Sistan and Baluchestan, Zahedan, Iran

ABSTRACT

In this paper, the effects of magnetization patterns on the performance of Hybrid Electrical Vehicle (HEV) are investigated. HEVs have three magnetic field sources: armature winding, permanent magnets, and field winding. To initiate the investigation, the magnetic field distributions produced by these three sources are obtained. By using the magnetic field distributions, the machine is analyzed under no-load and on-load conditions, and the operational indices, such as self and mutual inductance, cogging-, reluctance- and instantaneous torque, and unbalance magnetic force (UMF) in x- and y direction are calculated. Various magnetization patterns are considered to investigate their influences on the performance of the machine. This step was done with Maxwell software. Furthermore, instantaneous torque and magnitude of UMF are expressed in terms of pole arc to pole pitch ratio by using artificial intelligence. The optimal of the pole arc to pole pitch ratio to maximize the average of instantaneous torque and minimize the magnitude of UMF by some multi-objective algorithms is also computed. The modeling and optimization are performed by MATLAB Software.

Article Info

Keywords: Auxiliary winding, Hybrid excitation synchronous machine, Multi-objective optimization, Permanent magnet.
Article History:
Received 2021-07-14
Accepted 2021-09-23

I. INTRODUCTION

The permanent magnet synchronous machines (PMSMs) are widely used in industry due to their high efficiency and torque to volume ratio. Despite their advantages, their flux control capabilities are limited due to the constant permanent magnet flux, especially in surface-mounted PMSMs [1]. To overcome this weakness, it is recommended to use PMSMs with an auxiliary excitation. These machines are named hybrid excitation synchronous machines (HESMs). Therefore, they can be utilized as HEV. These machines have been used in propulsion applications [2] and three-wheel electrical vehicles [3]. Moreover, they can be equipped with a modular magnetic-shunting rotor [4].

HESMs are divided into two types: series HESMs (SHESMs) and parallel HESMs (PHESMs) [5-8]. In SHESMs, the magnet flux and the auxiliary winding (AW) flux pass through the same path, which leads to less iron losses [5]. The machines can operate in the flux-enhancing mode when the fluxes are in the same directions, and if the fluxes are in the opposite directions, the machine is in the flux-weakening mode of operation. In SHESMs, there is a higher probability of demagnetization because the whole AW flux passes through the magnet, and the flux controllability is reduced due to the low permanent magnet permeability [5], [7-8]. In PHESMs, the risk of demagnetization is reduced and, controllability is increased. However, the iron losses are increased because the flux routes of excitation sources are different [5], [8].

[†]**Corresponding Author**: a.hoseinpour@uoz.ac.ir
Tel: +98-9153409088, University of Zabol
Faculty of Electrical Engineering, University of Zabol, Zabol, Iran

If both field sources are placed in the stator, not only there is no need for retaining the sleeve but also the heat is easier removed. However, the mutual torque is not generated, and the end winding effects are considerable [9]. Some of the structures of the machine [10-11] limit the available space for the winding, so the diameter of the stator should be high. Therefore, the torque to volume ratio reduces [12].

If the magnet is on the rotor and the AW is in the stator, the reluctance and the mutual torque are produced. To reduce iron losses, the external rotor structure can be used [13].

If both field excitation sources are located on the rotor [14], mutual, and reluctance torque components are generated. This machine can be employed in constant power applications [12] with speed variations. However, the existence of brushes and retaining sleeves is the disadvantage of this structure [11].

Therefore, a series HESM in which both excitation sources are in the rotor is selected as HEV. Three structures are suggested that both of the rotor excitations are located in the rotor: spoke [15], buried [16], and surface mounted (SM) [17]. Among these three types, only the SM one is a series hybrid excitation synchronous machine, so it is chosen. The structure of a SHESM is shown in Fig. 1.

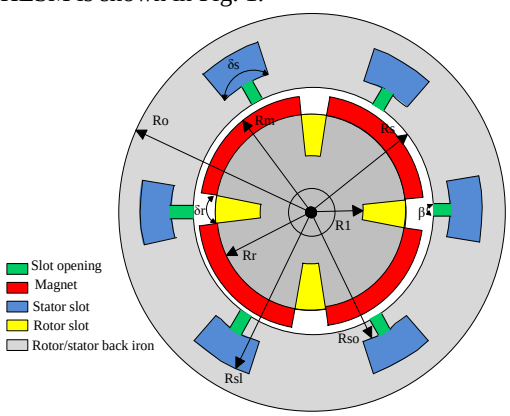


Fig 1. Configuration of SHESM.

Various types of magnetization patterns are reported for PMSMs [18] among which radial magnetization (RM), parallel magnetization (PM), and Halbach magnetization (HM) are more popular. The type of magnetization pattern highly influences the magnetic flux density distribution. Therefore, the performance of the machine is significantly affected by the magnetization pattern. HSEM has been analyzed with a parallel magnetization pattern in [17]. In the present paper, three types of magnetization (RM, PM, and HM) are considered, and the SHESM is analyzed for open-circuit and under load modes of operation.

To model the magnet, there are some methods, such as splitting the magnet into some pieces [19]. However, the Fourier series model was used in tangential and radial directions [20].

In addition, there are two different layouts for stator winding. The first one is non-overlapping, and the second one is overlapping. Moreover, the non-overlapping type is divided into alternate-teeth wounds and all-teeth wounds [20]. It is assumed that the armature winding is a non-overlapping alternate-teeth wound for the SHESM.

In this paper, first, the method of calculating the magnetic field has been explained for a magnetostatic. Then, the torque, inductance, and UMF have been determined for a rotating SHESM. To evaluate the effects of the magnetization pattern on the machine performances, three types of magnetization are simulated, and the results are compared. Finally, the influence of the pole arc to pole pitch ratio on torque and UMF is analyzed.

II. Analysis of SHESM

A. Calculation of flux density

Ampere and Gauss laws are used to obtain the magnetic field in the machine.

$$\nabla \times \boldsymbol{H} = \boldsymbol{J} \quad (1)$$

$$\nabla . \boldsymbol{B} = 0 \quad (2)$$

Where $\boldsymbol{J}$, $\boldsymbol{H}$, and $\boldsymbol{B}$ are current density, magnetic field intensity, and magnetic flux density, respectively.

Equation (3) states the relationship between $\boldsymbol{B}$ and $\boldsymbol{H}$ in the magnetized area.

$$\boldsymbol{B}=\mu_0\mu_{rm}\boldsymbol{H}+\mu_0\boldsymbol{M} \quad (3)$$

Where μ_0, μ_{rm}, and $\boldsymbol{M}$ are permeability of free space, the relative permeability of magnet, and magnetization vector, respectively.

Substituting relation (3) in the Ampere's law yields:

$$\nabla \times \boldsymbol{B} = \mu_0\mu_r\boldsymbol{J} + \mu_0\nabla \times \boldsymbol{M} \quad (4)$$

Where μ_r is the relative permeability of winding space. Given that the $\nabla.\boldsymbol{B} = 0$, thus flux density is Curl of another quantity which is called the vector magnetic potential. Therefore,

$$\boldsymbol{B} = \nabla \times \boldsymbol{A} \quad (5)$$

Replacing equation (5) in (4) and considering that $\nabla.\boldsymbol{A} = 0$, the following relation is obtained:

$$\nabla^2\boldsymbol{A} = -\mu_0\mu_r\boldsymbol{J} - \mu_0\nabla \times \boldsymbol{M} \quad (6)$$

In regions where there is current but no magnetization (e.g., winding regions), the following relation can be written.

$$\nabla^2\boldsymbol{A} = -\mu_0\mu_r\boldsymbol{J} \quad (7)$$

In regions where there is magnetization but no current (e.g., magnet), we will have the following relation.

$$\nabla^2\boldsymbol{A} = -\mu_0\nabla \times \boldsymbol{M} \quad (8)$$

In regions where there is neither current nor magnetization (e.g., air-gap region), the Laplace equation can be written.

$$\nabla^2\boldsymbol{A} = 0 \quad (9)$$

These equations are solved numerically in Maxwell software by finite element method [21]; thus flux density is calculated.

B. Energy calculation

The magnetic energy of a system is given by the following expressions. The expressions represent total values of energy for the volumes taken into account. Note that the integrals

have simpler expressions if the material property of the object considered is a linear one. In the case of linear material properties, magnetic energy and co-energy values are identical ($w = w_c$).

$$w = w_c = \int_V \left(\int_0^B \boldsymbol{H}.d\boldsymbol{B} \right) dV \tag{10}$$

where V is the volume of the machine.

C. UMF calculation

The radial and tangential forces are calculated by Maxwell stress tensor. First, the flux density should be computed then the mentioned magnetic pull is obtained by the following relations.

$$f_r = \frac{1}{2\mu_0}\left({B_r}^2 - {B_\theta}^2\right) \tag{11}$$

$$f_\theta = \frac{1}{\mu_0} B_r B_\theta \tag{12}$$

These equations can be transformed into the Cartesian system.

$$f_x = f_r \cos(\theta) - f_\theta \sin(\theta) \tag{13}$$

$$f_y = f_r \sin(\theta) + f_\theta \cos(\theta) \tag{14}$$

Then, the x- and y components of UMF are determined with the integration of these magnetic pulls in the middle of the air gap by formulas numbers (15) and (16). Finally, the magnitude of UMF is calculated based on them by (17).

$$F_x = \int_{-L/2}^{L/2} \int_{-\pi}^{\pi} f_x r \, d\theta \, dz = L \int_{-\pi}^{\pi} f_x r \, d\theta \tag{15}$$

$$F_y = \int_{-L/2}^{L/2} \int_{-\pi}^{\pi} f_y r \, d\theta \, dz = L \int_{-\pi}^{\pi} f_y r \, d\theta \tag{16}$$

$$F_r = \sqrt{F_x^2 + F_y^2} \tag{17}$$

D. Torque calculation

The instantaneous torque ($\boldsymbol{T_{inst}}$) is computed by $\boldsymbol{T} = \boldsymbol{r} \times \boldsymbol{F}$ as follows.

$$\boldsymbol{r} = r a_r$$

$$\boldsymbol{F} = F_r a_r + F_\theta a_\theta$$

$$T_{inst} = r \times F = (r a_r) \times \int_{-\frac{L}{2}}^{\frac{L}{2}} \int (f_r a_r + f_\theta a_\theta) \, dl \, dz = \frac{L}{\mu_0} \int r \, B_\theta B_r \, dl a_z \tag{18}$$

The instantaneous torque has three components. The first one is cogging torque, the second one is reluctance torque, and the last one is mutual torque. In order to compute cogging torque magnet and AW are active, and stator excitation is inactive. In contrast, just armature winding should be excited to calculate reluctance torque. Mutual torque is achieved by the interaction between field- and armature excitation.

E. Inductance calculation

The mutual inductance between two phases is computed by the following equation.

$$w_{ij} = \frac{1}{2} L_{ij} I^2 \rightarrow L_{ij} = \frac{2w_{ij}}{I^2} \tag{19}$$

Where w_{ij} is the energy stored in the magnetic field linking conductor i with conductor j. I is the current in conductor i. In order to set the self-inductance of a phase, just consider i instead of j as bellow

$$w_{ii} = \frac{1}{2} L_{ii} I^2 \rightarrow L_{ii} = \frac{2w_{ii}}{I^2} \tag{20}$$

III. SIMULATION RESULTS

A. MODELING OF SHESM

According to Fig. 3, the center of the magnet is aligned with the first slot of the stator, and the layout of the stator winding is an alternate-teeth wound. The characteristic of the machine is presented in Table I, and three types of magnetization for the magnets are considered. The machine's rotor moves in the dynamic analysis, and the torque, the mutual inductance of stator phases, and the UMF are calculated.

The spatial angle is chosen as the horizontal axis in the Figs of this section. In the following, inductance, torque, and UMF are computed for this machine.

The mutual inductances, between stator phases, are independent of the type of magnetization, and depend on the configuration of the stator coil and the machine dimensions. The individual flux linkage of each phase is more than the coupling flux with other phases; thus the self-inductance value is more than mutual inductances. Further, the stator self-inductance is a function of the rotor position because it includes a slot. Since the angle between phases is 120 degrees, so the two-phase mutual inductance is negative. These points are clearly visible in Fig. 4.

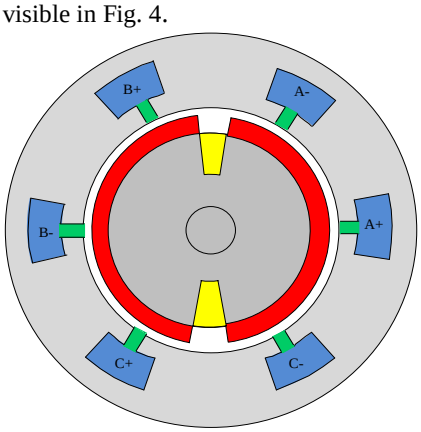


Fig. 3 The structure of SHESM.

TABLE I
Parameters of the SHESM.

Parameters	symbols	Values	Parameters	symbols	Values
Number of pole-pairs	p	1	Stator-slot span angle	δ_s	0.6283 rad
Number of stator-slots	Q_s	6	Stator-slot-opening span angle	β	0.4398 rad
Number of rotor-slots	Q_r	2	Rotor-slot span angle	δ_r	0.4712 rad
Outer radius of machine	R_o	105 mm	Pole arc to pole pitch ratio	α	0.85
Outer radius of the stator-slots	R_{sl}	81.5 mm	Permanent magnet remanence	B_{rem}	1 T
Outer radius of the stator-slot-opening	R_{so}	62.9 mm	Relative recoil permeability of magnets	μ_{rm}	1.05
Staor bore radius	R_s	57.5 mm	Cross sectional area of wire in stator and rotor	A_c	1.2 mm^2
Magnet Radius	R_m	56 mm	Rotor current	I_r	10 A
Rotor back-iron radius	R_r	50 mm	Stator peak current	I_m	14.14 A
Inner rotor-slot radius	R_1	26.5 mm	Number of stator coil winding turns	N_{ts}	422
Motor axial length	L	90 mm	Number of rotor coil winding turns	N_{tr}	212

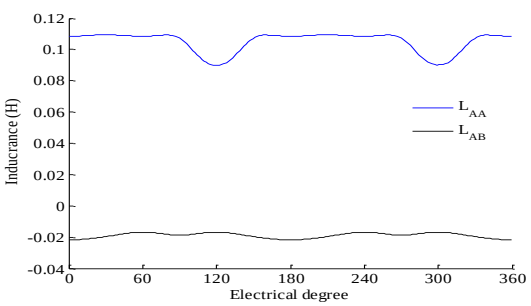


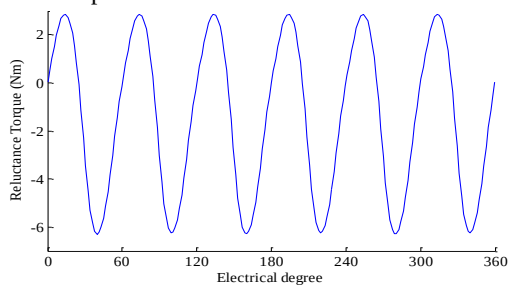
Fig.4. Self and mutual inductances.

The instantaneous torque includes three components; reluctance-, cogging-, and mutual torque. In this SHESM, the reluctance torque is produced by armature excitation; thus it is independent of the magnetization. Despite the reluctance torque, the cogging and mutual torque, in which the excitation resources of the field have the main influence, are affected by the magnetization type. Therefore, the instantaneous torque is affected by the magnetization patterns.

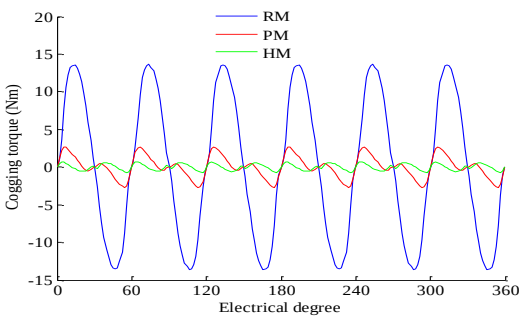
Reluctance torque is shown in Fig. 5.a. By comparison of the presented Figs for cogging torque in Fig. 5.b, HM has the lowest cogging torque, so from this point of view, it is more desirable.

The average amounts of T_{inst} for RM, PM, and HM are 34.68, 29.88, and 27.37 N.m., respectively. Therefore, radial magnetization produces higher torque, but it is not recommended for applications where the torque ripple is important.

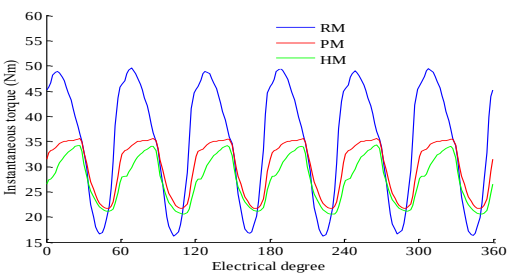
The unbalanced magnetic forces can be divided into two components along the x and y axes. The two components of three magnetization patterns are shown in Figs 6.a and 6.b. The magnitude of the force, which is calculated from equation 17 is shown in Fig. 6.c. It can be deduced from Fig. 6 that the HM produces less UMF.



a

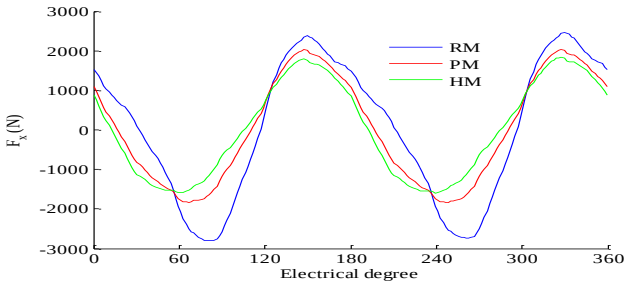


b

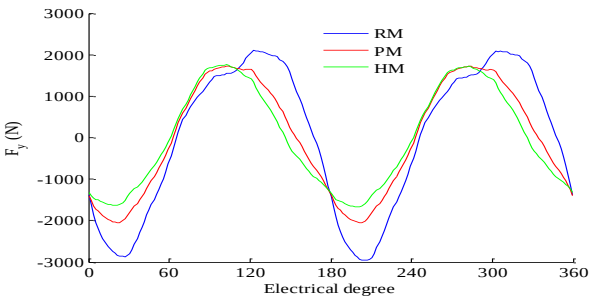


c

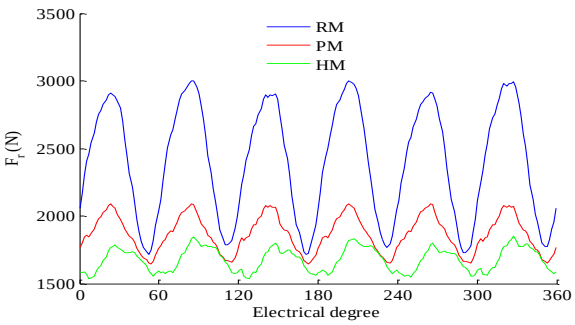
Fig.5. a) Reluctance torque. b) Cogging torque due to three magnetization patterns. c) Instantaneous torque for RM, PM, and HM.



a



b



c

Fig.6. a) UMF in x direction. b) UMF in y direction. c) The magnitude of UMF.

B. OPTIMAL DESIGN

In this section, the effect of the pole arc to pole pitch ratio on the SHESM performance, denoted by α, is investigated. Indeed, the impact of changes of α on the average instantaneous torque (T_{ave}) and the magnitude of UMF (F_r) are demonstrated. Magnet is the main field source, and rotor winding is the auxiliary field source which causes that α be greater than 0.5. Moreover, the magnetization type is considered to be RM, and rotor current density is constant.

Table.II presents T_{ave} for several values of α. As well, Fig.7 shows T_{ave} versus α, and it is clear that a second-degree polynomial can be fitted to it as follows

$$T_{ave} = -54.3571\alpha^2 + 74.0257\alpha + 10.9297 \quad \text{Nm} \qquad (21)$$

TABLE. II.
Average torque

α	0.95	0.85	0.75	0.65	0.55
T_{ave}	32.15	34.68	35.85	36.01	35.24

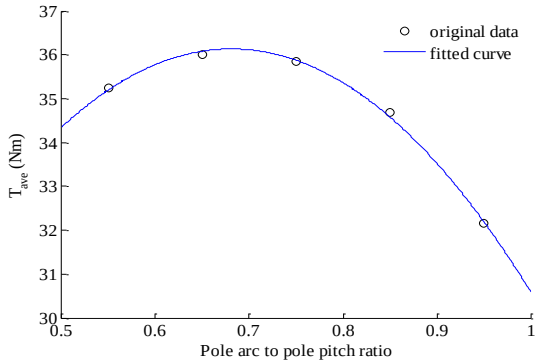


Fig. 7.T_{ave} versus α

According to equation (21) the maximum of the T_{ave} is achieved by α=0.6809 is 36.13. If SHESM is simulated by mentioned α the average torque is 36.07.

After that, the influence of pole arc to pole pitch ratio on the magnitude of UMF will be analyzed. According to Table.III, decreasing the value of α leads to decreasing in F_r average (F_{ra}). Therefore, from this point of view, the reduction of α is suitable. It can also be fitted grade 3 polynomial for the relation between F_{ra} with α as presented in (22)

$$F_{ra} = -21.1166\alpha^3 + 42.1964\alpha^2 - 25.2142\alpha + 6.3 \quad KN \qquad (22)$$

TABLE. III.
Changes of F_{ra} due to α

α	0.95	0.85	0.75	0.65	0.55
F_{ra}	2341	2416	2255	1986	1735

Now, two expressions obtained for the average torque and F_{ra}must be optimized simultaneously. Given that, the goal is to minimize, so instead of torque, its inverse is considered. In fact, we are faced with a two-objective optimization problem as follows:

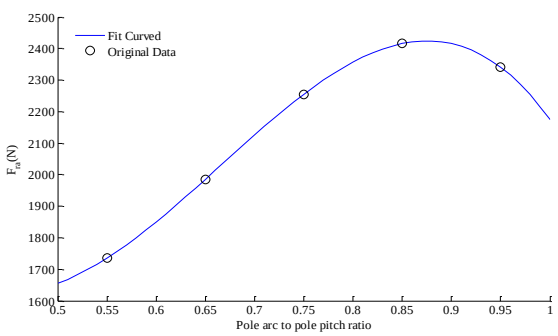


Fig. 8.pF_{ra} versus α

Min (1/Tave, Fr) (23)

$1/T_{ave}$=1/(-54.3571α^2+74.0257α+10.9297) (24)

F_r=-21.1166α^3+42.1964α^2-25.21421α+6.3 (25)

s.t 0.50<a<1 (26)

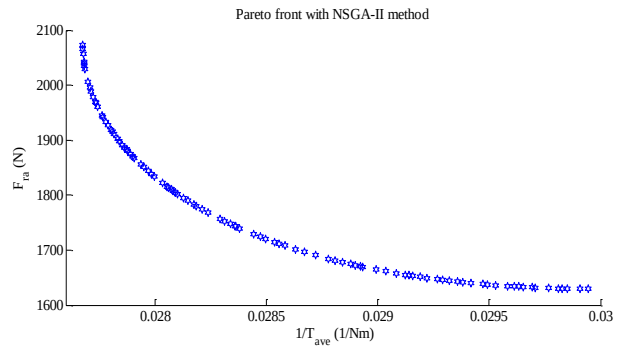
If the mentioned multi-objective problem is optimized with the NSGA-II, PESA-II, and MPSO algorithm, the obtained

Pareto fronts as shown in Fig. 9a to 9c. The results are very close, so the optimal point of Pareto front will be achieved by fuzzy Max-Min [22] algorithm in MPSO Pareto front, which is

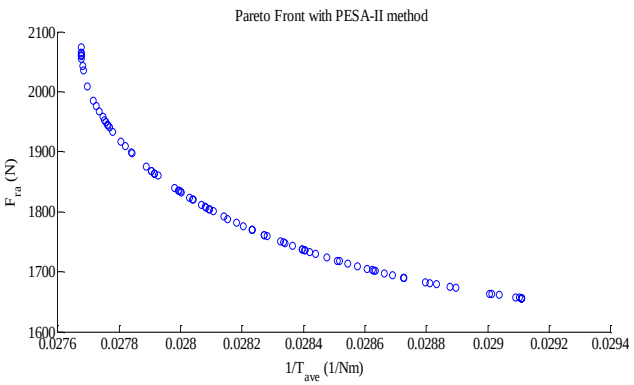
$$\alpha = 0.5335 \quad (27)$$

$$T_{ave} = \frac{1}{0.0286} = 34.965 \quad (28)$$

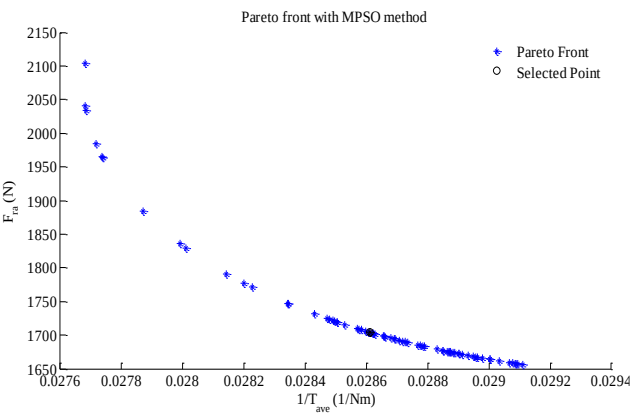
$$F_{ra} = 1702 \quad (29)$$



(a)



(b)



(c)

Fig. 9. Pareto front for both objective (magnitude of UMF and inverse of instantaneous torque) a) NSGA-II b) PESA-II c) MPSO

If the SHESM is simulated for obtained pole arc to pole pitch ratio, the instantaneous torque diagram will be as shown in Fig. 11. Furthermore, the curve of UMF in x - and y direction, and its magnitude are drowned in Fig11.

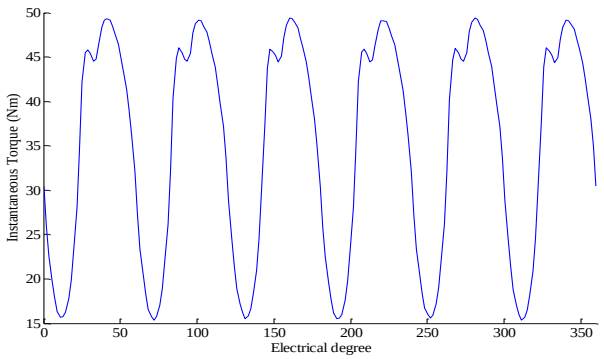


Fig. 10. Instantaneous torque

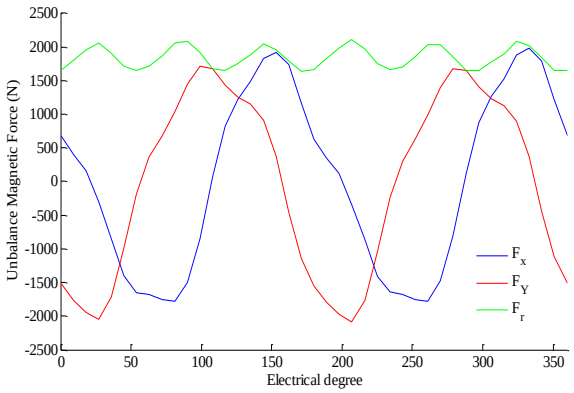


Fig. 11: Unbalance magnetic force

CONCLUSIONS

In this paper, a SHESM was introduced, and the effect of different magnetization patterns was evaluated on its performance. High average instantaneous torque is achieved with radial magnetization, while low cogging torque, torque ripple, and UMF are obtained with Halbach magnetization. Moreover, increasing average instantaneous torque and decreasing magnitude of UMF can be achieved by determining the pole pitch to pole are ratio properly.

REFERENCES

[1] A. Hosseinpour, M. Mardaneh and A. Rahideh "*Investigation of the Effects of Different Magnetization Patterns on the Performance of Series Hybrid Excitation Synchronous Machines*" Progress In Electromagnetics Research M, Vol. 64, 109–121, 2018.

[2] C. Wang, Z. Zhang, Y. Liu and H. Gao, "*Mechanical Design and Analysis of a High-Torque Modular Hybrid Ecitation Synchronous Machine for Electric Vehicle Propulsion Applications* "IEEE Transactions on Vehicular Technology, Vol. 69, Is. 9, 2020.

[3] A. Shah Mohammadi and J. P. F. Trovão, " *System-Level System-Level Optimization of Hybrid Excitation Synchronous Machines for a Three-Wheel Electric Vehicle* "IEEE Transactions on Transportation Electrification, Vol. 6, Is. 2, 2020.

[4] Y. Liu, Z. Zhang, C. Wang and H. Gao, "Optimization and Performance Improvement of a Hybrid Excitation Synchronous Machine with Modular Magnetic-Shunting Rotor", *IEEE Transactions on Industrial Electronics*, Vol. 67, Is. 6, 2020.

[5] Y. Amara, S. Hlioui, Rachid Belfkira, G. Barakat and M. Gabsi "Comparison of open circuit flux control capability of a series double excitation machine and a parallel double excitation machine" *IEEE Trans. Veh. Technol.*, vol. 60, no. 9, Nov 2011.

[6] Y. Wang and Z. Deng "Hybrid excitation topologies and control strategies of stator permanent magnet machines for DC power system" *IEEE Trans. Ind. Elec.*, vol. 59, no. 12, 2012.

[7] W. Geng, Z. Zhang, K. Jiang and Yangguang Yan, "A new parallel hybrid excitation machine: permanent-magnet/variable-reluctance machine with bidirectional field-regulating capability*" IEEE Trans. Ind. Elec.*, vol. 62, no. 3, Mar. 2015.

[8] K. Kamiev, J. Pyrh¨onen, J. Nerg,V. Zaboin and J. Tapia "Modeling and testing of an armature-reaction-compensated (PM) synchronous generator" *IEEE Trans. Energy Convers.*, vol. 28, no. 4, Dec. 2013.

[9] X. Zhu, M. Cheng, W. Hua, J. Zhang, and W. Zhao, "Design and analysis of a new hybrid excited doubly salient machine capable of field control," in *Conf. Rec. IEEE IAS Annu. Meeting*, Tampa, FL, USA, 2006, vol. 5,pp. 2382–2389.

[10] W. Hua, M. Cheng, and G. Zhang, "A novel hybrid excitation flux switching motor for hybrid vehicles," *IEEE Trans. Magn.*, vol. 45, no. 10,pp. 4728–4731, Oct. 2009.

[11] R. L. Owen, Z. Q. Zhu, and G. W. Jewell, "Hybrid-excited flux-switching permanent-magnet machines with iron flux bridges," *IEEE Trans. Magn.*, vol. 46, no. 6, pp. 1726–1729, Jun. 2010.

[12] Z. Zhang, S. Ma, J. Dai and Y. Yan "Investigation of Hybrid Excitation Synchronous Machines With Axial Auxiliary Air-Gaps and Non-Uniform Air-Gaps" *IEEE Trans. Ind Appl.*, vol. 50, no. 3, May/Jun. 2014.

[13] L. Xiaogang and T. A. Lipo, "A synchronous/permanent magnet hybrid AC machine," *IEEE Trans. Energy Convers.*, vol. 15, no. 2, pp. 203–210, Jun. 2000

[14] A. Hosseinpour, M. Mardaneh and A. Rahideh "Two-dimensional analytical model for double field excitation synchronous machines" IET Generation, Transmission & Distribution , Vol. 15, Is. 6, pp. 1081-1093, 2021.

[15] S. I. Kim, J. Cho, S. Park, T. Park and S. Lim "Characteristics comparison of a conventional and modified spoke-type ferrite magnet motor for traction drives of low-speed electric vehicles " *IEEE Trans. on Ind. Appl.*, vol. 49, no. 6, pp. 2516-2523, 2013.

[16] K. Kamiev, J. Nerg, J. Pyrhönen, V. Zaboin, and J. Tapia "Feasibility of an armature-reaction-compensated permanent-magnet synchronous generator in island operation" *IEEE Trans. Ind. Elec.*, vol. 61, no. 9, Sep. 2014.

[17] H. Bali, Y. Amara, G. Barakat, R. Ibtiouen and M. Gabsi "Analytical modeling of open circuit magnetic field in wound field and series double excitation synchronous machines" *IEEE Trans. Magn.*, vol. 46, no. 10, Oct. 2010.

[18] A. Rahideh , M. Mardaneh , and T. Korakianitis "Analytical 2-D Calculations of Torque, Inductance, and Back-EMF for Brushless Slotless Machines With Surface Inset Magnets" *IEEE Trans. Magn.*, Vol. 49, no. 8, pp.1-12, Aug. 2013.

[19] V. Z .Faradonbeh, A. Rahideh, M. M. Ghahfarokhi, E. Amiri, A. D. Aliabad, G.A Markadeh,"Analytical Modeling of Slotted, Surface Mounted Permanent Magnet Synchronous Motors with Different Rotor Frames and Magnet Shapes" IEEE Transactions on Magnetics, Vol. 57, Is. 1, 2021.

[20] A. Rahideh and T. Korakianitis, "Analytical magnetic field calculation of slotted brushless permanent-magnet machines with surface inset magnets," *IEEE Trans. Magn.*, vol. 48, no. 10, pp. 2633–2649, Oct.2012.

[21] M. Ghods, Z. Nasiri-Gheidari, and H. Oraee " Performance Analysis of Permanent Magnet Vernier Generator under Mechanical Faults" *International Journal of Industrial Electronics, Control and Optimization*, Vol. 1, No. 2, pp. 121-131, 2018.

[22] G. Xiao, T. Zhu, Y. Chen and X. Yang "*Linear Searching Method for Solving Approximate Solution to System of Max-Min Fuzzy Relation Equations With Application in the Instructional Information Resources Allocation*" IEEE ACCESS, vol. 7, pp. 65019-65028, 2019.



Alireza Hoseinpour was born in Zabol, Iran in 1985. He received his B.Sc. degree with honors from Sistan and Baluchestan University of Zahedan, Iran in 2007. In 2010, he received his M.Sc. degree from the Ferdowsi University of Mashhad, Iran and Ph.D. degree in 2018 from the Shiraz University of Technology all in electrical engineering. Following receipt of the Ph.D. degree, he joined the University of Zabol, Iran. His main research interests are wind turbine, renewable energy, permanent magnet synchronous machine drive, four-switch three-phase inverter, power electronic, and design of hybrid electrical vehicle.



Ahmad Khajeh was born in Zabol, Iran in 1982. He received the B.Eng. degree from Sistan and Baluchestan University, Zahedan, Iran, in 2004 and the M.Eng. and Ph.D. degrees from the Amirkabir University of Technology and Ferdowsi University of Mashhad, Iran in 2007 and 2014, all in electrical engineering, respectively. Currently, he is an Assistant Professor with the Faculty of Electrical and Computer Engineering, University of Sistan and Baluchestan, Zahedan, Iran. His current research interests include power electronics, wind power, adjustable speed drives, and photovoltaic system.

IECO

This page intentionally left blank.